PAPER

SERS profiling of blood serum filtrate components from patients with type II diabetes using 100 kDa filtration devices†

Zainub Shoukat,‡[a] Rafia Atta,‡[a] Muhammad Irfan Majeed, *[a] Haq Nawaz, *[a] Nosheen Rashid,[b] Abdulrahman Alshammari,[c] Norah A. Albekairi,[c] Aleena Shahzadi,[a] Sonia Yaseen,[a] Amna Tahir,[a] Yasmeen Naseer,[a] Aziz Fatima,[a] Rimsha Tahir,[a] Maria Ghafoor[a] and Saqib Ali[d]

Blood carries some of the most valuable biomarkers for disease screening as it interacts with various tissues and organs in the body. Human blood serum is a reservoir of high molecular weight fraction (HMWF) and low molecular weight fraction (LMWF) proteins. The LMWF proteins are considered disease marker proteins and are often suppressed by HMWF proteins during analysis. This issue is addressed by using a filtration device to isolate the filtrate portion from blood serum samples having biomarker proteins up to the size of the cutoff value of the filtration device. In this research, 100 kDa filter devices are employed to obtain the filtrate portions from blood serum samples of type II diabetes mellitus patients and healthy volunteers, followed by characterization using surface-enhanced Raman spectroscopy (SERS) with silver nanoparticles (Ag NPs) as the SERS substrate. By using this approach, the collected filtrate is expected to contain marker proteins at a size of <100 kDa, which are associated with type II diabetes. These marker proteins are in a narrow size range (cutoff value of 100 kDa). Hence, they may be more easily identified by their characteristic SERS spectral features as compared to their analysis in the respective whole blood serum samples due to the exclusion of larger size proteins. These proteins that are present in the filtrate portions of type II diabetes may include adiponectin, C-reactive protein, insulin, leptin, RBP4, IL-6, TNF-α, Fibroblast Growth Factor 21 (FGF21), albumin, transthyretin, alpha-antitrypsin, transferrin, apolipoprotein A-1 (ApoA-1) and fetuin-A. Some prominent SERS bands are observed at 356 cm⁻¹, 435 cm⁻¹, 490 cm⁻¹, 548 cm⁻¹, 596 cm⁻¹, 729 cm⁻¹, 746 cm⁻¹, 950 cm⁻¹, 1330 cm⁻¹, 1362 cm⁻¹, 1573 cm⁻¹ and 1689 cm⁻¹, which differentiate type II diabetes patients from healthy individuals. Moreover, the SERS spectral data sets of various samples are classified using two chemometric approaches: principal component analysis (PCA) and partial least square discriminant analysis (PLS-DA). The validation of the PLS-DA analysis classification model is indicated with 81% accuracy, 79% specificity, and 85% sensitivity, having a value of AUC = 0.75.

1. Introduction

Type II diabetes mellitus is a fast-growing global issue and a non-insulin-dependent metabolic disease[1] with social, economic and health-related outcomes.[2] The International Diabetes Federation has declared that it has become the 6th

*a*Department of Chemistry, University of Agriculture Faisalabad, Faisalabad, 38000, Pakistan. E-mail: haqchemist@yahoo.com; irfan.majeed@uaf.edu.pk

*b*Department of Chemistry, University of Education, Faisalabad Campus, Faisalabad, 38000, Pakistan

*c*Department of Pharmacology and Toxicology, College of Pharmacy, King Saud University, Post Box 2455, Riyadh, 11451, Saudi Arabia

*d*Département de Chimie, Faculté des Sciences et de Génie, Université Laval, Québec, QC G1V 0A6, Canada

† Electronic supplementary information (ESI) available. See DOI: https://doi.org/10.1039/d4ra06335j

‡ The first two authors contributed equally to this work.

leading cause of death across the world, as 537 million people are suffering from diabetes globally, and it has been predicted that extended figures will be 783 million in 2045.[3] Type II diabetes mellitus is a pancreatic inflammation that is marked by elevated blood glucose level due to inadequate production of insulin by pancreatic beta cells, which leads to hyperglycemia.[4] Due to insulin resistance, glucose (primary source of energy) is not taken up by tissues (muscles, liver and adipose tissues), which can cause energy depletion in the body. Increased hunger, thirst, frequent urination, exhaustion, hazy eyesight, and slow wound healing are some prevalent symptoms of the disease.[5] If severe, it can become a medical emergency.[6] Complications of chronic inflammation include cardiovascular disease,[7] possible amputations, hypertension, loss of vision, renal failure, and anomalies in lipoprotein metabolism.[8] It has been demonstrated that weight loss management (as obesity is a major contributing factor in insulin resistance) and physical

activity can retard the risk factors associated with the development of prediabetes to type II diabetes.[9,10] Different gold standard techniques, including oral glucose tolerance testing (OGTT), HbA1c and fasting plasma glucose (FPG), are routinely used diagnostic tools for the assessment and screening of type II diabetes mellitus.[11] These techniques have different limitations, including low specificity, poor analytical stability, and time-consuming procedures. The early detection of type II diabetes is crucial, as undiagnosed inflammation can be life-threatening. Therefore, new analytical techniques should be explored for the development of methods that can quickly detect this disease in a cost-effective way and with the least amount of sample preparation. Raman spectroscopy has great potential to identify fingerprints of the molecules. It can be employed for different bioanalyses utilizing biofluids; for example, blood urine and serum, in which biomarker proteins of the disease are expected to be present.[12] Raman spectroscopy may be used for the identification of biochemical changes associated with distinct biomarkers of different diseases, as it is very sensitive, reliable, less time-consuming, and a rapid analytical technique.[13] In body fluids, biomolecules like RNA/DNA, protein, and lipids are found in low concentration. Thus, weak Raman signals are produced from these biomolecules, hindering their identification.[14] To overcome this problem, surface-enhanced Raman spectroscopy (SERS) is applied, which helps to enhance the signals with the help of metallic nanoparticles (silver or gold).[15–17] The silver nanoparticles (Ag NPs) are considered to enhance the signal more strongly due to the greater surface plasmon effect as a result of the availability of high numbers of active sites.[18] Moreover, they are inexpensive and easier to synthesize than gold nanoparticles. SERS has been widely used for the characterization of different bacterial strains,[19–21] as well as for the identification of biomarkers of various diseases, such as breast cancer,[22,23] tuberculosis,[16,24] hepatitis B (HBV),[25] oral cavity cancer,[26] hepatitis C (HCV),[27] typhoid[28] and dengue fever.[29]

In the current study, filtrate fractions of diabetic type 2 patients and non-diabetic persons are obtained by using 100 kDa filtration devices. Blood is a reservoir of lipids, proteins and aliphatic hydrocarbons,[30] where high molecular weight fraction (HMWF) proteins are abundantly found alongside low molecular weight fractions (LMWF), which are most limited. The HMWF include proteins (50–60%) strongly dominating the lower molecular proteins, and related biomolecules like amino acids, nucleic acids and carbohydrates.[31] Notably, the LMWF proteins are considered as disease biomarkers. However, due to their abundance, the HMWF suppress these lower molecular weight fraction biomolecules. Hence, their detection is difficult. In order to overcome this challenge, HMWF and LMWF are separated by employing ultra-centrifugal filter devices having different molecular weight cut-offs.[32] In this study, ultrafiltration devices are used to obtain the type II diabetes biomarkers having molecular weights of less than 100 kDa in the filtrate portion, followed by SERS analysis to identify the SERS spectral characteristic properties of the type II diabetes biomarkers which are give in Table 1. The progression of type II diabetes may cause fluctuations in the biomolecules of blood, generally accompanied

Table 1 Description of type II diabetes blood serum protein biomarkers with a mass of less than 100 kDa

Type II diabetes biomarkers	Molecular weight	References
Adiponectin	30 kDa	41
C-reactive protein	25 kDa	42
Leptin	16 kDa	43
Insulin	5.8 kDa	44
RBP4	21 kDa	45
IL-6	26 kDa	46
TNF-α	17 kDa	47
Fibroblast growth factor 21 (FGF21)	22 kDa	48
Albumin	66 kDa	49
Transthyretin	55 kDa	50
Alpha-antitrypsin	45 kDa	51
Transferrin	79 kDa	52
Apolipoprotein A-1 (ApoA-1)	28 kDa	53
Fetuin-A	60 kDa	54 and 55

by the appearance of new biomolecules along with an increase or reduction in the specific biomolecules, which will be characterized by SERS technique.[33] Moreover, the two chemometric approaches, principal component analysis (PCA) and partial least square discriminant analysis (PLS-DA), are used for qualitative analysis and for the semi-quantitative discrimination, respectively, of the spectral data sets of the healthy *versus* diabetes-positive individuals. From a literature review performed during this research work, we have shown that no published study has employed surface-enhanced Raman spectroscopy for the characterization of filtrate sections of blood serum proteins of type II diabetes in the cutoff range of 100 kDa. Our study is unique in targeting type II diabetes biomarkers within the range of 100 kDa. Previous studies[34–37] have used SERS for the analysis of serum of type II diabetes, but none of them used 100 kDa filtration, which is of paramount importance because the majority of the protein biomarkers lie in this range. The filtration used in this study enhances the specificity and sensitivity of our analysis.

2. Materials and methods

2.1. Silver nanoparticles synthesis

A chemical reduction process is utilized to synthesize the silver nanoparticles that will be the substrate for SERS. To do this, 0.017 g of silver nitrate ($AgNO_3$) was added to 100 milliliters of deionized water in a beaker, and then the mixture was heated to 80–85 °C. After that, 0.025 g of 1% trisodium citrate ($Na_3C_6H_5O_7$) was added to the mixture and heated for an hour on a hot plate, while being continuously stirred with a magnetic stirrer. To synthesize gray-colored silver nanoparticles, the supernatants were removed by centrifuging the mixture for 7 minutes at 600 round per minute.[38]

2.2. Collection of blood samples of type II diabetes

Blood samples of non-diabetic (healthy) volunteers and diabetic individuals were collected from the District Headquarter Hospital Toba Tek Singh, Pakistan. For this study, a total of 50 samples (including 35 disease samples and 15 healthy samples)

were used. The blood samples were taken in EDTA/sodium fluoride tube, and centrifuged for 10 minutes at 2000 rpm to get blood serum. Furthermore, ultracentrifugation of serum samples using 100 kDa filter devices (Amicon Ultra-2 ml, Merck, Millipore) was performed at 6500 rpm for 30 minutes to concentrate the low molecular weight fractions termed as the filtrate portion against the high molecular weight fractions, which are called residue.[39]

2.3. SERS spectral measurements

SERS spectra were collected with a Peak Seeker Pro-785 Raman spectrometer (Agiltron, USA) equipped with a 785 nm diode laser. For each sample, 40 μl of filtrate portions from blood serum samples of diabetes positive and healthy volunteers were mixed with 40 μl of silver nanoparticles for an incubation period of 1 hour in Eppendorf tubes with a micropipette. After incubation, a sample mixture of 25 μl volume was placed on an aluminum slide with a groove *via* micropipette for SERS spectral acquisition. The laser power used for each sample was adjusted to 50 mW, and the integration time was 10 seconds. Using the same conditions for each sample, 15 SERS spectra were collected in the range of 400–1800 cm^{-1}.

2.4. Data preprocessing of the SERS spectra

The spectral features of SERS were pre-processed by using the MATLAB 7.8 software. The processing of spectra includes vector normalization, baseline correction, smoothing and background removal. The Savitzky Golay method and Rubber band were used for vector normalization and baseline removal, respectively.[40] The contribution from the aluminum slide substrate in the sample spectra was removed by subtraction method.

2.5. Multivariate data analysis

Multivariate data analysis methods like PCA and PLS-DA were employed to compare the SERS spectra obtained from the filtrate parts of blood serum from healthy controls and type II diabetic patients after filtration with the 100 kDa devices. A large number of uncorrelated variables can be reduced to a smaller number of correlated variables by utilizing PCA, an unsupervised statistical method. Reducing the dimensions, in which the first principal component (PC-1) explained the major variations in the spectral features and the second principal component (PC-2) described the remaining variation, preserves the changes in the spectral features. By excluding the orthogonal dimensions for data variability, loadings of PC are utilized to classify the SERS spectral features sets of different samples employed in this study. The false positive rate for specificity and the true positive rate for sensitivity are explained by the ROC curve, and PLS-DA is a supervised method that can be used to calibrate, validate, predict, and categorize the high-dimension SERS spectral data sets exhibiting variability.

3. Results and discussions

Human serum is a reservoir of HMW and LMW fractions, in which 99% of the serum part is taken up by highly abundant

proteins. These proteins suppress less abundant proteins, which are potentially disease biomarkers that can be mined for disease biomarker identification by ultracentrifugation of the serum (kDa), followed by SERS analysis.

3.1. Mean SERS spectra of whole serum *versus* filtrate portion of diabetic samples

Fig. 1 depicts the mean SERS spectra of the diabetic whole serum and the filtrate portion from the same sample of blood serum. It clearly shows the spectral differences that appear due to centrifugation and the elimination of larger proteins weighing more than 100 kDa. This helps to distinguish the variations taking place during the progression of type II diabetes. Certain SERS spectral features that are not seen in the mean spectrum of the filtrate, but observed in the whole serum, are caused by the presence of HMWF. These SERS features include the bands at 575 cm^{-1} (C–C bending vibration in phosphatidylinositol), 841 cm^{-1} (C–C bending vibration in glucose), 957 cm^{-1} (PO_4^{3-}), 1330 cm^{-1} (phospholipids region linked with DNA) and 1654 cm^{-1} (C=C lipid stretch) represented by solid lines. Similarly, the SERS bands that appeared in the filtrate portion but were absent in the whole serum are indicated by solid lines, and include the features at 383 cm^{-1} (skeletal vibrational modes in proteins), 746 cm^{-1} (breathing mode of ring of thymidine in DNA) 1075 cm^{-1} (symmetric stretching vibration of ν_3 PO_4^{3-}), 1275 cm^{-1} (amide III), 1540 cm^{-1} (vibrations of the carbonyl group of the amide and aromatic hydrogen) and 1323 cm^{-1} (stretching vibrations in guanine (B, Z-marker)). These SERS bands appeared in the filtrate portion due to the abundance caused by filtration (100 kDa) of LMW fraction, which can be considered disease biomarkers. The SERS spectral features that are present in the spectra of both diabetic whole serum and its filtrate portion, but differ in their intensities, are denoted by dashed lines. A sharp peak present at 456 cm^{-1} caused by ring deformation vibrations in L-tryptophan (protein) has low intensity in the whole serum samples, but slightly increased intensity in the filtrate samples. A high intensity peak present in the whole serum samples is present at 729 cm^{-1} (ring bending mode in L-histidine), but the intensity is reduced in the filtrate portion. A SERS band at 1100 cm^{-1} (fatty acids and n(C–C)-lipids) with medium intensity appeared in the whole serum sample, but decreases in the filtrate sample. A low intensity peak present at 1398 cm^{-1} is caused by the (C=O symmetric stretching) in the whole serum samples, but exhibits further reduced intensity in the centrifuged samples (filtrate). Similarly, a prominent peak appeared at 1448 cm^{-1}, indicating the presence of CH_2CH_3 deformation. The filtrate samples show medium intensity, which decreases in the unfiltered samples. This occurs due to the prominence of the corresponding component upon eliminating the HMW fractions. Significantly, the peaks appearing in the SERS spectra of the filtrate samples result from the removal of the high molecular weight fraction weighing more than 100 kDa. These peaks were not present in the whole serum sample due to the predominance of the larger proteins.
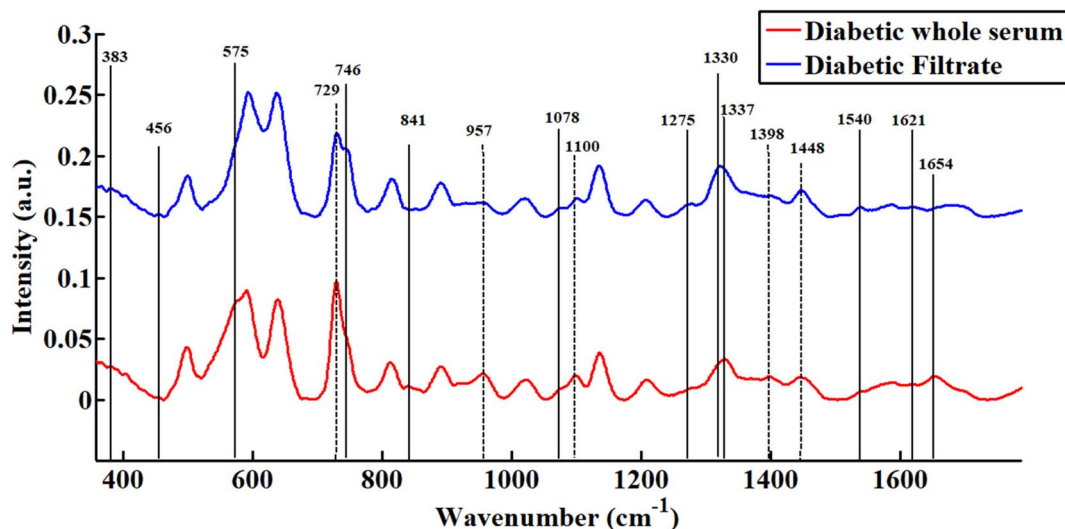
Fig. 1 Mean plot of SERS spectra for the uncentrifuged (whole serum) and centrifuged (filtrate) type II diabetic serum samples.

3.2. Mean SERS spectra of the filtrate portions of diabetes-positive and healthy individual blood serum samples

Fig. 2 shows all the mean features of the filtrate portions of blood serum samples from patients with type II diabetes and healthy individuals. The solid lines highlight specific peaks that are absent in one spectrum but present in other spectra, indicating key differences in the molecular signatures between the samples. The peaks that are present in both spectra, but exhibit an increasing or declining trend of intensity, are represented by dotted lines. The SERS properties, including the bands at 421 cm^{-1} (skeletal bending mode in proteins), 490 cm^{-1} (C–O–C; glycosidic bond in glycogen), 812 cm^{-1} (Z-marker of phosphodiester), 860 cm^{-1} (PO_4^{3-}), 920 cm^{-1} (C–C stretching within the proline ring), 957 cm^{-1} (phosphate group), 1215 cm^{-1} (C–N stretching), 1259 cm^{-1} (C–H in-plane bending in thymine),

1337 cm^{-1} bending motion of methylene from the backbone (glycine & proline), 1590 cm^{-1} (breathing vibrations in tryptophan) and 1783 cm^{-1} (carbonyl group in lipid contents (fatty acids & triglycerides)), are visible in the healthy individuals only and absent in the spectra of the diabetic samples. The SERS bands appearing at 500 cm^{-1} (torsional movement around C–OH_3 of the methoxy group), 686 cm^{-1} (C–N bending vibration in glycine), 746 cm^{-1} (ring breathing mode of thymidine in DNA), 950 cm^{-1} (C–C stretching vibrations for the proline and valine (proteins)), 1180 cm^{-1} (C–N in-plane bending in cytosine), 1330 cm^{-1} (phospholipids region linked with DNA), 1362 cm^{-1} (guanine (N7, B, Z-marker)), 1573 cm^{-1} (C=C stretching vibration in guanine) and 1689 cm^{-1} (amide I (unarranged structure; non-hydrogen bonded)) are observed only in the filtrate fractions (100 kDa) of blood serum samples from the diabetic patients, and could be regarded as disease markers.
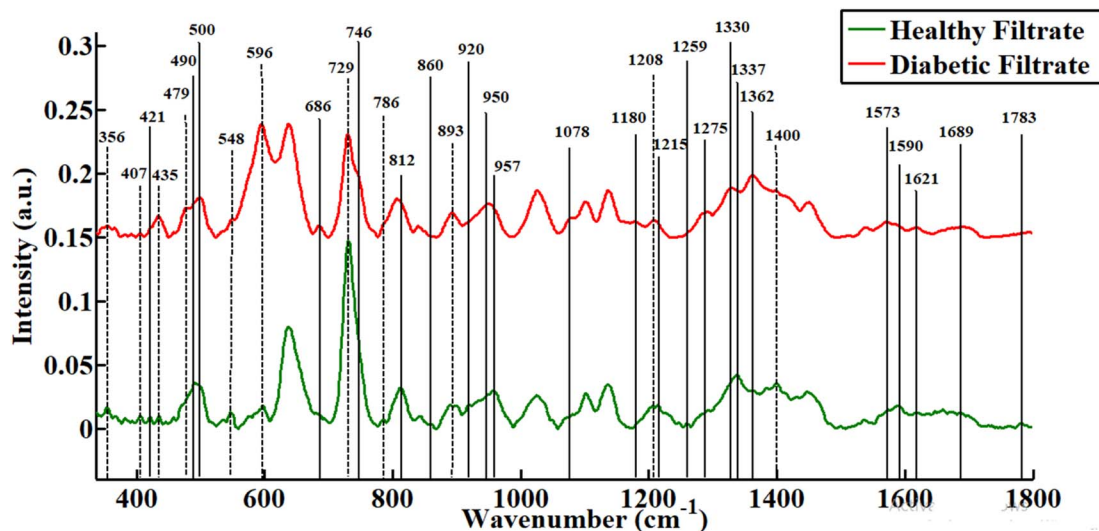

Fig. 2 Mean plot of the SERS spectra for the filtrate portions of healthy individuals and type II diabetic patients' blood serum samples.

Table 2 SERS peak assignments of spectral characteristics collected by 100 kDa devices from filtrate sections of healthy volunteers and type II diabetic persons

SERS peaks (cm^{-1})	Peak assignments	References
356	Vibrational mode of (C–C–C) glucose's ring	56
383	Skeletal vibrational modes in proteins	57
407	C–O–C bending in α-D-glucose	58
421	Skeletal bending mode in proteins	59
435	Lattice vibration in methylmyristic acid	58
456	Ring deformation vibrations in L-tryptophan (protein)	60
479	C–N–C bending in thymine	58
490	(C–O–C; glycosidic bond) in glycogen	61
500	Torsional movement around $C–OH_3$ of methoxy group	60
548	Skeletal bending vibration of the sterol ring in cholesterol	62
575	C–C bending vibration in phosphatidylinositol	62
596	C–C stretching vibration in phosphatidylinositol	62
686	C–N bending vibration in glycine	58
729	Ring bending mode in L-histidine	58
746	Breathing mode of ring of thymidine in DNA	63
786	Phosphate backbone (O–P–O stretching)	12 and 64
812	Phosphodiester (Z-marker)	65
841	C–C bending vibration in glucose	64
860	Phosphate group	62
893	Backbone, carbon–carbon skeletal	63
920	C–C stretching within the proline ring	61, 64 and 66
950	C–C stretching vibrations for the proline and valine (proteins)	67
957	PO_4^{3-}	57
1075	Symmetric stretching vibration of $\nu_3 PO_4^{3-}$	68
1078	Stretching vibration around ν(C–C) and ν(C–O) of phosphate group of phospholipids	69
1100	Fatty acids & n(C–C)-lipids	70
1180	C–N (in-plane bending) in cytosine	65
1208	C–C stretching or C–N stretching in lipids	57
1215	C–N stretching	71
1259	C–H in-plane bending in thymine	72
1275	Amide III	73
1292	Bending vibration in cytosine	65
1323	Stretching vibration in guanine (B, Z-marker)	65
1330	Phospholipids region linked with DNA	64, 74 and 75
1337	Bending motion of methylene from backbone (glycine & proline)	63 and 76
1362	Guanine (N7, B, Z-marker)	65
1398	C=O symmetric stretching	77
1400	In-plane deformation of NH	12
1448	CH_2–CH_3 deformation	68
1540	Vibrations of carbonyl group of amide and aromatic hydrogen	78
1573	C=C stretching vibration in guanine	61
1590	Breathing vibrations in tryptophan	79
1621	Indole ring stretching vibrations in tryptophan	68
1654	C=C lipid stretching	64
1689	Amide I (unarranged structure; non-hydrogen bonded)	73
1783	Carbonyl group in lipid content (fatty acids & triglycerides)	80

Some SERS bands are seen in healthy and in type II diabetes samples, including bands at 356 cm^{-1} (vibrational mode of (C–C–C) glucose's ring), 407 cm^{-1} (C–O–C bending in α-D-glucose), 435 cm^{-1} (lattice vibration in methylmyristic acid), 479 cm^{-1} (C–N–C bending in thymine), 548 cm^{-1} (skeletal bending vibration of the sterol ring in cholesterol), 596 cm^{-1} (C–C stretching vibration in phosphatidylinositol), 729 cm^{-1} (ring bending in L-histidine), 786 cm^{-1} (phosphate backbone (O–P–O) stretching), 893 cm^{-1} (backbone, C–C skeletal), 1078 cm^{-1} (stretching vibration of ν(C–C) & ν(C–O) of the phosphate group of phospholipids), 1208 cm^{-1} (C–C stretching or C–N stretching

in lipids), 1400 cm^{-1} (NH in-plane deformation) and 1292 cm^{-1} (bending vibration in cytosine). All of the above SERS features are shown in Table 2 with references from the literature. We have provided enlarged images (Fig. S3†) of the SERS mean plot of the healthy and diabetic filtrate samples in the ESI.†

3.3. Principle component analysis (PCA)

Multivariate SERS spectral data of healthy and type-2 diabetes patients are analyzed using principal component analysis (PCA). The unsupervised chemometric method reduces the dimensionality and complexity of the data, while producing

additional variables (PCs) for qualitative classification analysis. The first PCA dimension is PC-1, which is located on the *x*-axis, and PC-2, which is located on the *y*-axis of the PCA scatter plot, and provides the PCA loadings as the source of variance.

In this study, all the SERS spectral datasets of the healthy control and diabetes-positive patients were analyzed by PCA. It can effectively identify the changes among the SERS spectral datasets by minimizing the data complexity. The PCA scatter map of the SERS spectra of the filtrate portions of the centrifuged serum samples from both type II diabetics and healthy individuals is displayed in Fig. 3. PC-1 describes several SERS spectral clusters for various classes. The SERS spectra of the diabetic samples are depicted by red colored dots, whereas the spectra of the healthy samples are depicted by green colored dots, each of which represents a single SERS spectrum. In the PCA scatter plot (Fig. 3), where diabetic samples are grouped on the positive region of PC-1 and the spectra of the healthy samples are clustered on the negative side, there is a clear distinction between the SERS spectra of these two classes of filtrate parts from the blood serum samples. PC-1 accounts for the largest variance (52.30%) of the SERS spectra of the two sample groups in these SERS spectral datasets, while PC-2 accounts for 24.84% of the variance.

Fig. 4 displays the SERS spectral data sets of the filtrate parts of the healthy and type II diabetes serum samples. The negative loadings explain the SERS spectra of the healthy individuals that are grouped on the negative axis of the scatter plot (Fig. 3), while the positive-axis loadings are linked to the SERS spectra of the type II diabetes-positive samples that are aggregated on the positive axis. The PC loadings, also known as correlation coefficient vectors between the variables, offer an explanation of the underlying relationship between the original variables. The negative loadings of PC-1 associated with the SERS spectral datasets of healthy centrifuged serum samples are seen at 490 cm^{-1} (C–O–C; glycosidic bond in glycogen), 729 cm^{-1} (ring

bending mode in L-histidine), 860 cm^{-1} (PO$_4$$^{3-}$), 920 cm^{-1} (C–C stretching within the proline ring), 957 cm^{-1} (PO$_4$$^{3-}$), 1337 cm^{-1} bending motion of methylene from the backbone (glycine & proline) and 1783 cm^{-1} (carbonyl group in the lipid content). The PC-1 positive loadings are related to the diabetes-positive centrifuged serum samples, which are seen at 435 cm^{-1} (lattice vibration in methylmyristic acid), 479 cm^{-1} (C–N–C bending in thymine), 596 cm^{-1} (C–C stretching vibration in phosphatidylinositol), 893 cm^{-1} (backbone, C–C skeletal), 1078 cm^{-1} (stretching vibration around ν(C–C) and ν(C–O) of the phosphate group of phospholipids), 1180 cm^{-1} (C–N in-plane bending in cytosine), 1292 cm^{-1} (bending vibration in cytosine) and 1362 cm^{-1} (guanine (N7, B, Z-marker)). These findings demonstrate that the filtrate portion of the blood serum samples from the type II diabetes and non-diabetic individuals could be distinguished depending on the SERS spectral variations.

3.4. Partial least square discriminant analysis (PLS-DA)

Partial least square discriminant analysis (PLS-DA) is a statistical analysis tool used for discriminative modeling along with variable selection. To construct the relationship between the predictor and response variable, this model makes use of latent variables that help to categorize the SERS spectra of different samples into distinct classes, such as diabetes and healthy ones in the current study. For unbiased results, matrices of the overall SERS spectral data are constructed and then randomized. SERS spectral datasets are grouped into two categories, with 60% of the spectra randomly chosen for the calibration set and 40% of the spectral data selected for validation. Eight latent variables were selected in order to build the PLS-DA model. The Leave One Sample (15 SERS spectra) Out cross-validation method (LOOCV) is used in the validation technique. The filtrate parts of the healthy and diabetic serum samples get separated by score plot, as shown in Fig. 5.
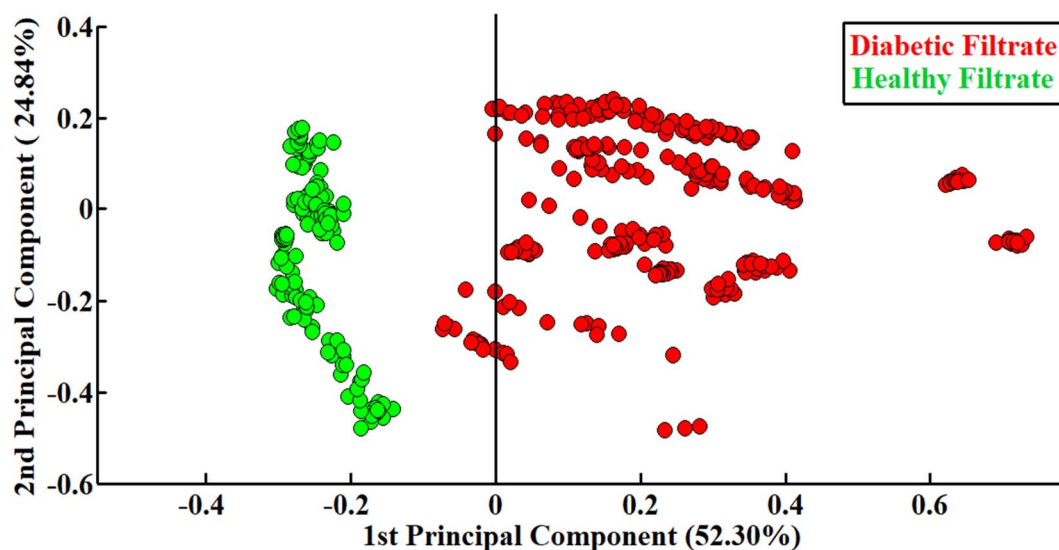

Fig. 3 PCA scatter diagram from the SERS spectra of the filtrate parts for centrifuged serum samples obtained from healthy and type II diabetes patients.
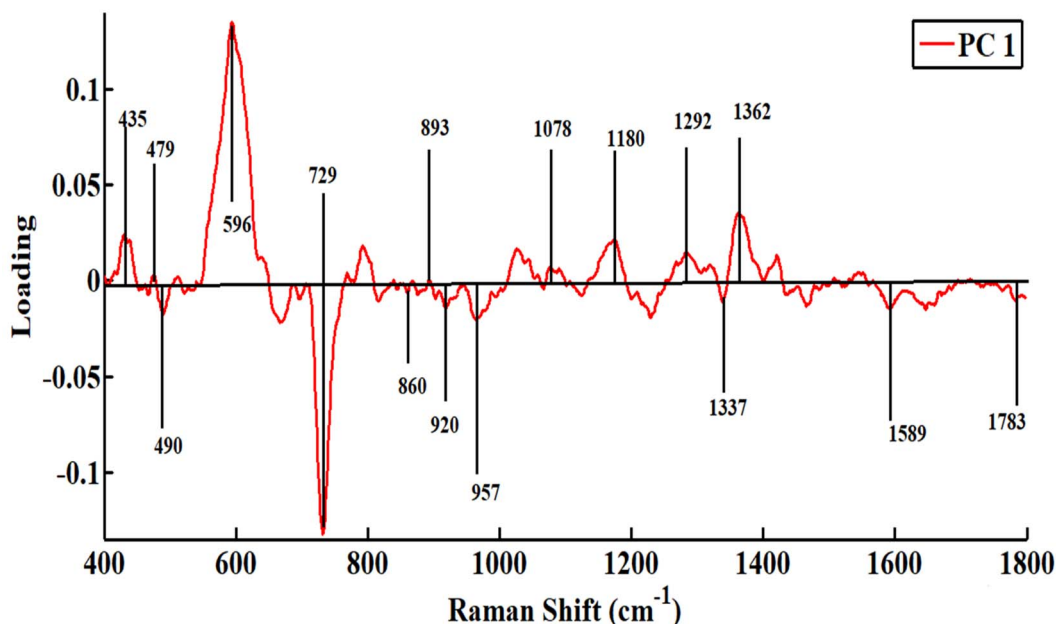
Fig. 4 PCA loadings of the SERS spectra from the filtrate parts of centrifuged serum samples from healthy and type II diabetes patients.

It is evident that the diabetic samples' spectrum datasets are classified on the positive side of the *x*-axis, whereas the healthy samples' spectral datasets are clustered on the negative side. The disease-positive samples' SERS spectra are displayed as red color dots, whereas the healthy samples' spectra are shown as green color dots. Fig. 6 shows the receiver operating curve (ROC) of the PLS-DA analysis, which further indicates how well this classification model can separate the SERS spectra of the type II diabetes patients from those of healthy individuals. As seen in Fig. 6, the value taken from the area under the curve (AUC) is

0.75. The 100% validity of the proposed model is shown by an AUC value of 1, whereas a value of zero renders the model null and void. The PLS-DA model has demonstrated 81% accuracy, 79% specificity, and 85% sensitivity in validation of the classification, indicating its reliability in classifying both diabetic and healthy samples.

3.5. Discussion

A prominent SERS band solely observed in the filtrate parts (SERS spectra) belonging to the healthy and type II diabetes
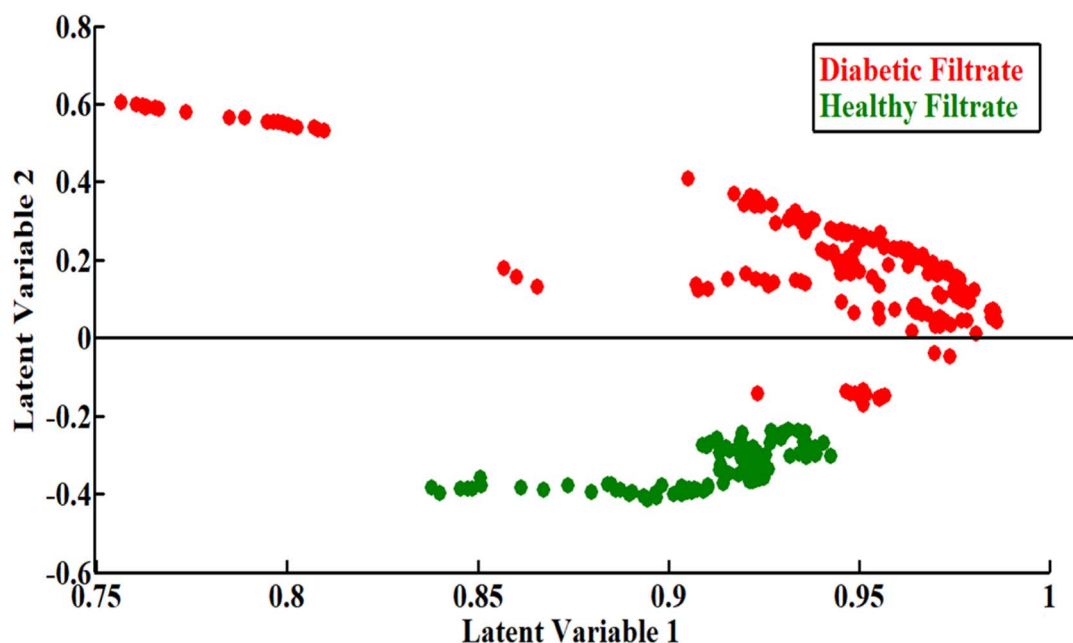

Fig. 5 PLS-DA model describing the classification of the SERS spectra of filtrates from the healthy and type II diabetes patients.
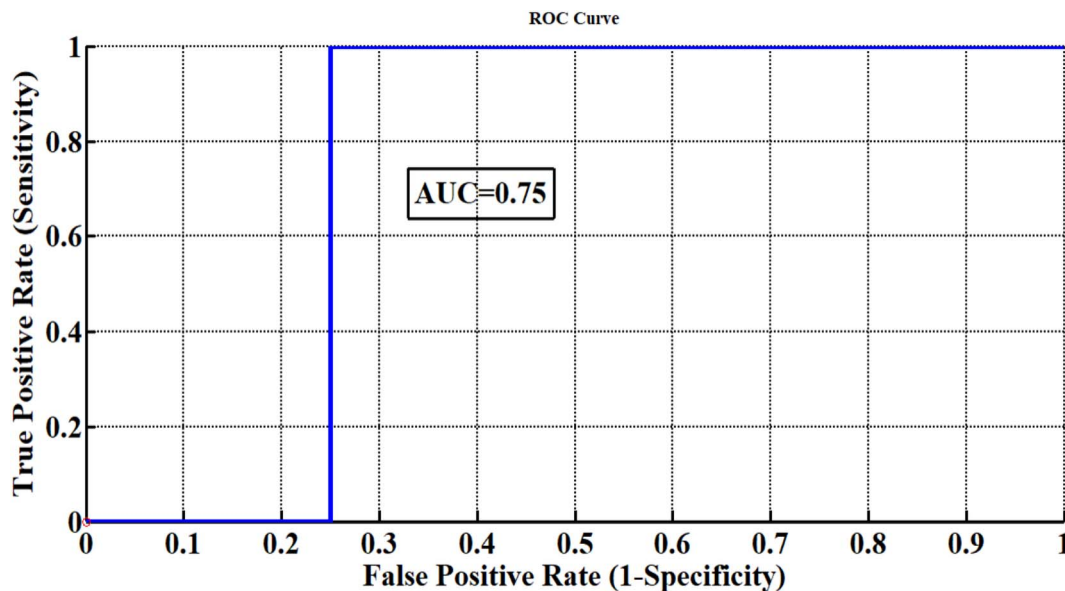
Fig. 6 Receiver operating curve (ROC) of the PLS-DA model to discriminate the filtrate sections of both type II diabetes patients and healthy individual's SERS spectra.

patients is observed at 1330 cm^{-1} and associated with phospholipids, which are linked to the increased blood glucose. It is critical to explore how the abundance of phospholipid contents alter the fatty acids patterns in type II diabetes mellitus patients, leading to obesity.[81] A prominent peak at 490 cm^{-1} is caused by glycogen, which is observed only in healthy samples, but not seen in disease samples. This indicates that there is reduced glycogen levels in the diabetic patients. It is important to note that glycogen is critically needed for the proper regulation of blood glucose levels.[82] The peak associated with amide I at 1689 cm^{-1} is only observed in the spectra from diabetic samples, and can be considered as a potential biomarker for the identification of the metabolic disease. The amide I peak indicates the altered protein conformations and impaired glucose metabolism.[83] The peaks present at 746 cm^{-1}, 1180 cm^{-1}, 1362 cm^{-1} and 1573 cm^{-1} are indicative of RNA/DNA bases (adenine, cytosine and guanine), which reflect their involvement in gene expression by the process of epigenetic modifications.[84] The peaks appearing at 356 cm^{-1} and 407 cm^{-1} with greater intensity in the disease samples as compared to the healthy ones can be associated with glucose, which may also be considered as a potential biomarker for the diagnosis of type II diabetes mellitus.[85] Another intense peak at 435 cm^{-1} in the diabetic samples indicates the high proportion of methyl myristic acid, which is a specific form of fatty acids. Diabetic patients have high cholesterol levels, which is indicated by the SERS band at 548 cm^{-1}.[86] Furthermore, in the diabetic samples, a high intensity peak at 596 cm^{-1} is due to phosphatidylinositol (combination of fatty acids, inositol (a sugar like molecule) and glycerol), which causes impaired glucose metabolism in the muscle cells.[87] The ʟ-histidine (observed at 729 cm^{-1}) is an essential amino acid required for metabolic activities (glucose metabolism) in the body, and appears with low intensity in the disease samples. A high intensity peak at 1078 cm^{-1} in the

diabetic patients as compared to non-diabetic ones is due to phospholipids, which is a saturated fatty acid responsible for increasing glucose production in the liver (hyperglycemia).[88] Moreover, all SERS bands from the filtrate parts of the diabetes patient samples may be taken as potential indicators for the detection of diabetes, resulting from the elevated levels of blood glucose.

4. Conclusions

Surface-enhanced Raman spectroscopy with Ag-nanoparticles as a SERS substrate, coupled with chemometric tools including principal component analysis (PCA) and partial least square discriminant analysis (PLS-DA), is found to be an excellent method for the rapid screening of type II diabetes mellitus patients with high 79% specificity and 85% sensitivity. The SERS technique is found to be useful for discriminating the SERS spectral features of the filtrate portions (obtained by using 100 kDa filtration devices) of the blood serum samples obtained from healthy volunteers and patients with type II diabetes. The major differentiating SERS spectral features related to type II diabetes and healthy persons are observed at 356 cm^{-1}, 407 cm^{-1}, 435 cm^{-1}, 490 cm^{-1}, 548 cm^{-1}, 596 cm^{-1}, 729 cm^{-1}, 746 cm^{-1}, 1078 cm^{-1}, 1330 cm^{-1}, 1362 cm^{-1}, 1573 cm^{-1} and 1689 cm^{-1}. It can be concluded that SERS is promising non-invasive technique, which offers valuable insights for the quick diagnosis of type II diabetes (pancreatic inflammation), particularly by using 100 kDa filtration devices for the blood serum samples. This additional step is helpful in acquiring the filtrate parts of the samples having <100 kDa protein biomarkers associated with type II diabetes. As these marker proteins are in a narrow size range (cutoff value 100 kDa), their identification *via* characteristic SERS spectral features can be achieved more easily from the filtrate, as compared to their

analysis in the respective whole blood serum samples, due to the exclusion of larger size proteins.

Ethical statement

This study was performed in strict accordance with the NIH guidelines for the protection of human subjects (45 CFR 46), and was approved by the Institutional Ethical Review Board (IERB) of Nishtar Medical University Multan, Pakistan (Reference No. 2230, dated 02-02-24). Informed consent was obtained from all human subjects.

Data availability

All data underlying the results are available as part of the article, and no additional source data are required.

Author contributions

Zainub Shoukat: writing – original draft; Rafia Atta: writing – review & editing; Muhammad Irfan Majeed: Supervision; Haq Nawaz: investigation, conceptualization; Nosheen Rashid: methodology; Abdulrahman Alshammari: funding acquisition; Norah A. Albekairi: resources; Aleena Shahzadi: validation; Sonia Yaseen: visualization; Amna Tahir: data curation; Zanib Javid: data curation; Aziz Fatima: software; Rimsha Tahir: software; Maria Ghafoor: formal analysis; Yasmeen Naseer: formal analysis.

Conflicts of interest

The authors have no known competing financial interests or personal relationships that could have appeared to influence the work reported in this paper.

Acknowledgements

References

1 U. Ehsan, H. Nawaz, M. I. Majeed, N. Rashid, Z. Ali, A. Zulfiqar, A. Tariq, M. Shahbaz, L. Meraj and I. Naheed, *Spectrochim. Acta, Part A*, 2023, **293**, 122457.

2 K. Kaul, J. M. Tarr, S. I. Ahmad, E. M. Kohner and R. Chibber, *Diabetes: an Old Disease, a New Insight*, 2013, pp. 1–11.

3 P. Saeedi, I. Petersohn, P. Salpea, B. Malanda, S. Karuranga, N. Unwin, S. Colagiuri, L. Guariguata, A. A. Motala and K. Ogurtsova, *Diabetes Res. Clin. Pract.*, 2019, **157**, 107843.

4 A. Berbudi, N. Rahmadika, A. I. Tjahjadi and R. Ruslami, *Curr. Diabetes Rev.*, 2020, **16**, 442–449.

5 T. Drivsholm, N. de Fine Olivarius, A. Nielsen and V. Siersma, *Diabetologia*, 2005, **48**, 210–214.

6 R. Silbert, A. Salcido-Montenegro, R. Rodriguez-Gutierrez, A. Katabi and R. G. McCoy, *Curr. Diabetes Rep.*, 2018, **18**, 1–16.

7 P. Steg, D. Karila-Cohen and L. Feldman, *Arch. Mal. Coeur Vaiss. Prat.*, 2000, **93**, 19–24.

8 A. D. Association, *Diabetes Care*, 2010, **33**, S62–S69.

9 A. R. Shuldiner, R. Yang and D.-W. Gong, *N. Engl. J. Med.*, 2001, **345**, 1345–1346.

10 A. D. Association, *Diabetes Care*, 2020, **43**, S89–S97.

11 R. G. Barr, D. M. Nathan, J. B. Meigs and D. E. Singer, *Ann. Intern. Med.*, 2002, **137**, 263–272.

12 S. Farquharson, C. Shende, F. E. Inscore, P. Maksymiuk and A. Gift, *J. Raman Spectrosc.*, 2005, **36**, 208–212.

13 M. Tahira, H. Nawaz, M. I. Majeed, N. Rashid, S. Tabbasum, M. Abubakar, S. Ahmad, S. Akbar, S. Bashir and M. Kashif, *Photodiagn. Photodyn. Ther.*, 2021, **34**, 102329.

14 S. Rafiq, M. I. Majeed, H. Nawaz, N. Rashid, U. Yaqoob, F. Batool, S. Bashir, S. Akbar, M. Abubakar and S. Ahmad, *Spectrochim. Acta, Part A*, 2021, **259**, 119908.

15 C. Fan, Z. Hu, A. Mustapha and M. Lin, *Appl. Microbiol. Biotechnol.*, 2011, **92**, 1053–1061.

16 K. Shahzad, H. Nawaz, M. I. Majeed, R. Nazish, N. Rashid, A. Tariq, S. Shakeel, A. Shahzadi, S. Yousaf and N. Yaqoob, *Anal. Lett.*, 2022, **55**, 1731–1744.

17 L. Zeiri, B. V. Bronk, Y. Shabtai, J. Eichler and S. Efrima, *Appl. Spectrosc.*, 2004, **58**, 33–40.

18 F. A. McClary, S. Gaye-Campbell, A. Y. Hai Ting and J. W. Mitchell, *J. Nanopart. Res.*, 2013, **15**, 1442.

19 A. Mushtaq, H. Nawaz, M. I. Majeed, N. Rashid, M. Tahir, M. Z. Nawaz, K. Shahzad, G. Dastgir, R. Z. A. Bari and A. ul Haq, *Spectrochim. Acta, Part A*, 2022, **278**, 121315.

20 S. Bashir, H. Nawaz, M. I. Majeed, M. Mohsin, S. Abdullah, S. Ali, N. Rashid, M. Kashif, F. Batool and M. Abubakar, *Photodiagn. Photodyn. Ther.*, 2021, **34**, 102280.

21 S. Bashir, H. Nawaz, M. I. Majeed, M. Mohsin, A. Nawaz, N. Rashid, F. Batool, S. Akbar, M. Abubakar and S. Ahmad, *Spectrochim. Acta, Part A*, 2021, **258**, 119831.

22 H. Hajab, A. Anwar, H. Nawaz, M. I. Majeed, N. Alwadie, S. Shabbir, A. Amber, M. I. Jilani, H. F. Nargis and M. Zohaib, *Spectrochim. Acta, Part A*, 2024, **311**, 124046.

23 S. Akbar, M. I. Majeed, H. Nawaz, N. Rashid, A. Tariq, W. Hameed, S. Shakeel, G. Dastgir, R. Z. A. Bari and M. Iqbal, *Anal. Lett.*, 2022, **55**, 1588–1604.

24 A. Kamran, A. Naman, M. I. Majeed, H. Nawaz, N. Alwadie, N. ul Huda, T. Tabussam, A. Bano, H. Hajab and R. Razaq, *RSC Adv.*, 2024, **14**, 8548–8555.

25 F. Batool, H. Nawaz, M. I. Majeed, N. Rashid, S. Bashir, S. Akbar, M. Abubakar, S. Ahmad, M. N. Ashraf and S. Ali, *Spectrochim. Acta, Part A*, 2021, **255**, 119722.

26 A. Amber, H. Nawaz, H. N. Bhatti and Z. Mushtaq, *Photodiagn. Photodyn. Ther.*, 2023, **42**, 103607.

27 S. Nasir, M. I. Majeed, H. Nawaz, N. Rashid, S. Ali, S. Farooq, M. Kashif, S. Rafiq, S. Bano and M. N. Ashraf, *Photodiagn. Photodyn. Ther.*, 2021, **33**, 102152.

28 M. Akram, M. I. Majeed, H. Nawaz, N. Rashid, M. R. Javed, M. Z. Ali, A. Raza, M. Shakeel, H. M. ul Hasan and Z. Ali, *Photodiagn. Photodyn. Ther.*, 2022, **40**, 103199.

29 T. Mahmood, H. Nawaz, A. Ditta, M. Majeed, M. Hanif, N. Rashid, H. Bhatti, H. Nargis, M. Saleem and F. Bonnier, *Spectrochim. Acta, Part A*, 2018, **200**, 136–142.

30 L. Sennels, M. Salek, L. Lomas, E. Boschetti, P. G. Righetti and J. Rappsilber, *J. Proteome Res.*, 2007, **6**, 4055–4062.

31 M. Leeman, J. Choi, S. Hansson, M. U. Storm and L. Nilsson, *Anal. Bioanal. Chem.*, 2018, **410**, 4867–4873.

32 D. R. Parachalil, C. Bruno, F. Bonnier, H. Blasco, I. Chourpa, J. McIntyre and H. J. Byrne, *Analyst*, 2019, **144**, 4295–4311.

33 S. Kumar, T. Verma, R. Mukherjee, F. Ariese, K. Somasundaram and S. Umapathy, *Chem. Soc. Rev.*, 2016, **45**, 1879–1900.

34 H. Han, X. Yan, R. Dong, G. Ban and K. Li, *Appl. Phys. B*, 2009, **94**, 667–672.

35 J. L. González-Solís, J. R. Villafan-Bernal, B. Martínez-Zérega and S. Sánchez-Enríquez, *Lasers Med. Sci.*, 2018, **33**, 1791–1797.

36 S. K. Das, T. S. Bhattacharya, M. Ghosh and J. Chowdhury, *New J. Chem.*, 2021, **45**, 2670–2682.

37 J. Lin, Z. Huang, S. Feng, J. Lin, N. Liu, J. Wang, L. Li, Y. Zeng, B. Li and H. Zeng, *J. Raman Spectrosc.*, 2014, **45**, 884–889.

38 H. Fang, X. Zhang, S. J. Zhang, L. Liu, Y. M. Zhao and H. J. Xu, *Sens. Actuators, B*, 2015, **213**, 452–456.

39 F. Bonnier, G. Brachet, R. Duong, T. Sojinrin, R. Respaud, N. Aubrey, M. J. Baker, H. J. Byrne and I. Chourpa, *J. Biophotonics*, 2016, **9**, 1085–1097.

40 H. Nawaz, F. Bonnier, P. Knief, O. Howe, F. M. Lyng, A. D. Meade and H. J. Byrne, *Analyst*, 2010, **135**, 3070–3076.

41 f. f. M. Fisher, M. Trujillo, W. Hanif, A. Barnett, P. G. McTernan, P. Scherer and S. Kumar, *Diabetologia*, 2005, **48**, 1084–1087.

42 O. Asbaghi, F. Fouladvand, M. J. Gonzalez, V. Aghamohammadi, R. Choghakhori and A. Abbasnezhad, *Complement. Ther. Med.*, 2019, **46**, 210–216.

43 W. Mohammed Saeed and D. Nasser Binjawhar, *Diabetes, Metab. Syndr. Obes.: Targets Ther.*, 2023, 2129–2140.

44 L. D. Roberts, A. Koulman and J. L. Griffin, *Lancet Diabetes Endocrinol.*, 2014, **2**, 65–75.

45 A. Cabre, I. Lazaro, J. Girona, J. Manzanares, F. Marimon, N. Plana, M. Heras and L. Masana, *J. Int. Med.*, 2007, **262**, 496–503.

46 A. D. Pradhan, J. E. Manson, N. Rifai, J. E. Buring and P. M. Ridker, *JAMA*, 2001, **286**, 327–334.

47 G. Kumar, D. Ponnaiyan, H. Parthasarathy, A. Tadepalli and S. Veeramani, *Genet. Test. Mol. Biomarkers*, 2020, **24**, 431–435.

48 Y. C. Woo, C. H. Lee, C. H. Fong, A. Xu, A. W. Tso, B. M. Cheung and K. S. Lam, *Clinical Endocrinology*, 2017, **86**, 37–43.

49 P. A. C. Freitas, L. R. Ehlert and J. L. Camargo, *Arch. Endocrinol. Metab.*, 2017, **61**, 296–304.

50 X. Hu, Q. Guo, X. Wang, Q. Wang, L. Chen, T. Sun, P. Li, Z. Shan, L. Liu and C. Gao, *Nutrients*, 2022, **14**, 2953.

51 V. M. Lindley, K. Bhusal, L. Huning, S. N. Levine and S. K. Jain, *J. Am. Coll. Nutr.*, 2021, **40**, 98–103.

52 J. Dai Kim, D.-M. Lim, K.-Y. Park, S. E. Park, E. J. Rhee, C.-Y. Park, W.-Y. Lee and K. W. Oh, *Endocrinol. Metab.*, 2020, **35**, 610.

53 L. Gao, Y. Zhang, X. Wang and H. Dong, *BMC Endocr. Disord.*, 2021, **21**, 1–11.

54 S. Rasul, A. Ilhan, M. H. Reiter, J. Todoric, S. Farhan, H. Esterbauer and A. Kautzky-Willer, *Clinical Endocrinology*, 2012, **76**, 499–505.

55 M. Hermans, V. Brandenburg, M. Ketteler, J. Kooman, F. Van der Sande, E. Boeschoten, K. Leunissen, R. Krediet, F. Dekker and Netherlands cooperative study on the adequacy of Dialysis, *Kidney Int.*, 2007, **72**, 202–207.

56 S. Sharma, R. Uttam, A. S. Bharti, N. Shukla and K. N. Uttam, *Natl. Acad. Sci. Lett.*, 2019, **42**, 365–368.

57 Z. Movasaghi, S. Rehman and I. U. Rehman, *Appl. Spectrosc. Rev.*, 2007, **42**, 493–541.

58 J. De Gelder, K. De Gussem, P. Vandenabeele and L. Moens, *J. Raman Spectrosc.*, 2007, **38**, 1133–1147.

59 T. G. Spiro, *Biological Applications of Raman Spectroscopy*, Wiley, 1987.

60 H. Schulz and M. Baranska, *Vib. Spectrosc.*, 2007, **43**, 13–25.

61 N. Stone, C. Kendall, N. Shepherd, P. Crow and H. Barr, *J. Raman Spectrosc.*, 2002, **33**, 564–573.

62 C. Krafft, L. Neudert, T. Simat and R. Salzer, *Spectrochim. Acta, Part A*, 2005, **61**, 1529–1535.

63 J. W. Chan, D. S. Taylor, T. Zwerdling, S. M. Lane, K. Ihara and T. Huser, *Biophys. J.*, 2006, **90**, 648–656.

64 N. Stone, C. Kendall, J. Smith, P. Crow and H. Barr, *Faraday Discuss.*, 2004, **126**, 141–157.

65 A. Ruiz-Chica, M. Medina, F. Sánchez-Jiménez and F. Ramirez, *J. Raman Spectrosc.*, 2004, **35**, 93–100.

66 C. J. Frank, R. L. McCreery and D. C. Redd, *Anal. Chem.*, 1995, **67**, 777–783.

67 M. Gniadecka, H. Wulf, N. Nymark Mortensen, O. Faurskov Nielsen and D. H. Christensen, *J. Raman Spectrosc.*, 1997, **28**, 125–129.

68 W. T. Cheng, M. T. Liu, H. N. Liu and S. Y. Lin, *Microsc. Res. Tech.*, 2005, **68**, 75–79.

69 Z. Huang, A. McWilliams, H. Lui, D. I. McLean, S. Lam and H. Zeng, *Int. J. Cancer*, 2003, **107**, 1047–1052.

70 Z. Huang, H. Lui, D. I. McLean, M. Korbelik and H. Zeng, *Photochem. Photobiol.*, 2005, **81**, 1219–1226.

71 D. Naumann, Infrared and NIR Raman spectroscopy in medical microbiology, in *Infrared spectroscopy: new tool in medicine*, 1998, SPIE, vol. 3257, pp. 245–257.

72 M. Deluca, H. Hu, M. N. Popov, J. Spitaler and T. Dieing, *Commun. Mater.*, 2023, **4**, 78.

73 G. Shetty, C. Kendall, N. Shepherd, N. Stone and H. Barr, *Br. J. Cancer*, 2006, **94**, 1460–1464.

74 P. G. Andrus and R. D. Strickland, *Biospectroscopy*, 1998, **4**, 37–46.

75 R. Malini, K. Venkatakrishna, J. Kurien, K. M. Pai, L. Rao, V. Kartha and C. M. Krishna, *Biopolymers*, 2006, **81**, 179–193.

76 R. K. Dukor, *Handbook of Vibrational Spectroscopy*, 2006.

77 E. O. Faolain, M. B. Hunter, J. M. Byrne, P. Kelehan, M. McNamara, H. J. Byrne and F. M. Lyng, *Vib. Spectrosc.*, 2005, **38**, 121–127.

78 B. R. Wood, M. A. Quinn, B. Tait, M. Ashdown, T. Hislop, M. Romeo and D. McNaughton, *Biospectroscopy*, 1998, **4**, 75–91.

79 H. Takeuchi, *Biopolymers*, 2003, **72**, 305–317.

80 D. Kaushik and B. Michniak-Kohn, *AAPS PharmSciTech*, 2010, **11**, 1068–1083.

81 F. Jannasch, G. Bedu-Addo, M. B. Schulze, F. P. Mockenhaupt and I. Danquah, *Nutr. J.*, 2017, **16**, 63.

82 O. Kotoulas, S. Kalamidas and D. Kondomerkos, *Pathol., Res. Pract.*, 2006, **202**, 631–638.

83 C. F. Deacon, A. Plamboeck, S. Møller and J. J. Holst, *Am. J. Physiol. Endocrinol. Metab.*, 2002, **282**, E873–E879.

84 R. Holliday and J. E. Pugh, *Science*, 1975, **187**, 226–232.

85 J. Y. Kim, S. F. Michaliszyn, A. Nasr, S. Lee, H. Tfayli, T. Hannon, K. S. Hughan, F. Bacha and S. Arslanian, *Diabetes Care*, 2016, **39**, 1431–1439.

86 A. Basu, P. Basu, S. Morris and T. J. Lyons, in *Biomarkers in Cardiovascular Disease*, ed. V. B. Patel and V. R. Preedy, Springer Netherlands, Dordrecht, 2016, pp. 653–672, DOI: 10.1007/978-94-007-7678-4_49.

87 J. Long, Z. Yang, L. Wang, Y. Han, C. Peng, C. Yan and D. Yan, *BMC Endocr. Disord.*, 2020, **20**, 174.

88 Y. Y. Tham, Q. C. Choo, T. S. T. Muhammad and C. H. Chew, *Mol. Biol. Rep.*, 2020, **47**, 9595–9607.